IEEE Access
Multidisciplinary | Rapid Review | Open Access Journal

Received February 12, 2020, accepted February 23, 2020, date of publication March 17, 2020, date of current version June 5, 2020.

Digital Object Identifier 10.1109/ACCESS.2020.2981417

Path Tracking Control for Active Rear Steering Vehicles Considering Driver Steering Characteristics

HAN ZHANG, BO HENG, AND WANZHONG ZHAO
College of Energy and Power Engineering, Nanjing University of Aeronautics and Astronautics, Nanjing 210016, China

Corresponding author: Wanzhong Zhao (zwz@nuaa.edu.cn)

This work was supported in part by the National Key Research and Development Program of China under Grant 2017YFB0103604, in part by the Key Research and Development Plan of Jiangsu Province under Grant BE2018124, in part by the Funding for Outstanding Doctoral Dissertation in NUAA under Grant BCXJ17-03, and in part by the Postgraduate Research and Practice Innovation Program of Jiangsu Province under Grant KYCX17_0239.

ABSTRACT In this paper, a path tracking control for active rear steering vehicles considering driver steering characteristics is proposed to help drivers track the desired vehicle trajectory in a tailored way. Firstly, the driver model is established, and based on the driver steering data, the driver parameters are identified by the least square method. Based on driver model parameter identification, driver and vehicle models are formed for the MPC controller design. In MPC controller design, global objective function, considering the task performance, vehicle stability, driver's physical workloads, mental workloads and actuator performance, is designed to optimize the overall performance of the driver-vehicle system. On the constraint, the driver operating limit, actuator physical limit and vehicle stability performance limit are also considered to make the controller feasible to in the real practice. Simulation results under different conditions show that the controller can significantly improve the system performance and reduce the driver's workloads.

INDEX TERMS Path tracking, vehicle dynamics, active steering, model predictive control.

I. INTRODUCTION

In real driving scenario, vehicles can be affected by various external disturbances, such as road interference, surrounding obstacles, drivers' distractions or capability limits, and *et al.* Trajectory tracking is a significant issue in advanced driver assistant system and intelligent driving technology, such as lane keeping assistance (LKA), collision avoidance (CA), automatic parking (AP), and et al [1]–[7]. Most of these technologies are implemented by tracking a pre-planned qualified trajectory. For example, it is supposed that the LKA should help vehicle run near the central line of the road or within an expected driving zone [8]. The CA system will detect the obstacles around vehicles and then generate a safe trajectory, avoiding contact and collision between vehicles and obstacles [9]. The AP system should design a trajectory based on the vehicle surroundings and the current location, helping drivers to park properly [7].

Numerous studies related to trajectory tracking have been reported. In existing research, active steering has been considered as an effective way for vehicles to track the desired path. A path planning and stability control of CA system is designed by Wang to improve vehicle driving safety [9]. In this study, the active front steering was implemented and the additional steering angle was used as the control input to the system. The model parameter uncertainty as well as system interferences are considered, so a robust tracking controller is used to calculate the additional steering angle to track the pre-planned CA trajectory. Salehpour presented a vehicle path tracking by integrated chassis control [10]. In order to follow the desired path, linear quadratic regulator controller was developed to regulate direct yaw moment and corrective steering angle on wheels. Lin, Jiao and Wang proposed a path tracking strategy for a farm vehicle based on active disturbance rejection control technique and particle swarm optimization algorithm [11]. Similarly, active front steering was adopted to track the desired yaw angle, which can be calculated according to the difference between real path and pre-defined path.

Different from current active steering approaches, rear active steering is an emerging way to improve steering stability [12]–[14]. While steering at low speed, the rear wheel

The associate editor coordinating the review of this manuscript and approving it for publication was Rui Xiong.

steering angle can be adjusted in the opposite direction of the front wheels to reduce the steering radius. When steering at a high speed, the rear wheel steering angle can be regulated in the same direction of the front wheels in order to prevent oversteer and side slip accidents. A mechanical integral steering system was proposed in [15], which was focused on the steering box of the rear wheels, i.e. a cam-based mechanism. This new steering system aimed to improve the vehicle stability and handling performances by adopting an integral steering law, which was designed in terms of correlation between the steering angles of front and rear wheels. A control scheme through integration of direct yaw moment and active rear steering was developed in [16] to enhance vehicle stability. The required yaw moment and rear steering angle were calculated in the upper-level control structure by sliding mode controller and the yaw moment was achieved in the lower-level control structure by distributing the brake torques of each wheel appropriately. The active rear steering also can be used to accomplish the rollover prevention. In [17], a pulsed active rear steering control scheme was investigated to reduce the likelihood of rollover for motor vehicles. Based on rollover estimator, an on/off switch controller was used to active the rear steering system.

The control objectives of all the abovementioned research studies are mainly focused on path tracking or active steering technology. For a driver assistant technology, providing appropriate assistance to help drivers fulfill the driving task is the core content. While in the real driving scenarios, drivers will manipulate the steering wheel and pedals to adjust vehicle motions. In the meantime, ADAS will generate control inputs to vehicles according to vehicle driving states to improve vehicle stability and safety. The driver's reaction may vary from person to person since it is affected by many individual factors, such as driving experience, gender, habits, etc. [11]–[14], [18]–[21], so it is of great importance to consider drivers' characteristics in the design of ADAS. These individual differences have a significant impact on the driving performance [15], [22].

In order to help drivers track a desired path as well as improve the vehicle stability, an active rear steering control strategy considering drivers' characteristics is developed in this paper. Firstly, based on the driver steering data, the driver model can be identified. Based on driver model parameter identification, driver and vehicle models are formed for the MPC controller design. In MPC controller design, global objective function, considering the task performance, vehicle stability, drivers' physical workloads, mental workloads and actuator performance, is designed to optimize the overall performance of the driver-vehicle system. The driver operating limit, actuator physical limit and vehicle stability limit are also added to the controller solution as constrains to make the controller feasible in the real practice.

The rest of this paper is organized as follows. Section II gives a brief description of system modeling. The individualized control method based on MPC is designed in Section III. Simulation studies based on a CarSim® vehicle model are presented in Section IV, followed by some concluding remarks in Section V.

II. DRIVER-VEHICLE SYSTEM MODELING

In this section, the human driver model, vehicle model and driver-vehicle system are established for later controller design.

A. DRIVER MODEL

In the driving process, drivers manipulate the steering wheel according to the lateral displacement deviation between preview point of the desired path and vehicle predicted position, which can be described by driver steering models [23].

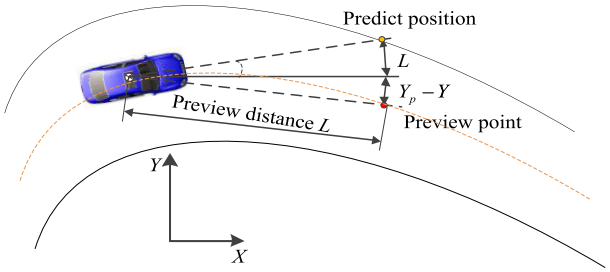

FIGURE 1. Schematic view of preview driver model.

As shown in Fig. 1, this lateral displacement deviation can be described as

$$\Delta Y(s) = Y_d(s)\, e^{\tau_p s} - Y(s) - L\varphi(s) \tag{1}$$

where $Y_d(s)\, e^{\tau_p s}$ stands for the lateral displacement of the desired path preview point and τ_p is the preview time; L denotes the preview distance which can be approximated as $v_x(s)\,\tau_p$; $v_x(s)$ is the longitudinal velocity; $\varphi(s)$ and $Y(s)$ stand for the current vehicle heading angle and lateral displacement, respectively. Therefore, $Y(s)+L\varphi(s)$ describes the lateral displacement of the predicted position for the vehicle at time $t + \tau_p$. The driver's steering wheel angle to track desired path can be simplified as a first-order driver model with lead-lag elements and time delay [30], [31]. Thus the driver model can be described as

$$\theta_{sw}(s) = \frac{G_h\,(1+\tau_L s)\, e^{-\tau_{d1} s}}{1+\tau_{d2} s}\Delta Y(s) \tag{2}$$

where $\theta_{sw}(s)$ is the driver's steering angle; G_h is the steering proportional gain; τ_{d1} and τ_{d2} are the pure delay time and the delay time constant representing driver's response, respectively; τ_L is the derivative time constant.

Usually, τ_L and τ_{d1} are significantly less than 1s. Therefore, $1 + \tau_L s$ can be considered as the approximation of $e^{\tau_L s}$. $(1 + \tau_L s)\Delta Y(s)$ can be approximated as the lateral displacement deviation between the preview point of the desired path and the predicted position of the vehicle at time $t + \tau_L + \tau_p$. In addition, the pure time-delay $e^{-\tau_{d1} s}$ can be approximated as $1/(1 + \tau_{d1} s)$. With above approximations, in order to facilitate the design of the controller, the driver model can

be rewritten in the form of differential equations as:

$$\begin{aligned}\ddot{\delta}_{sw} = &\frac{-1}{\tau_{d1}\tau_{d2}}\delta_{sw} - \frac{T_d}{\tau_{d1}\tau_{d2}}\dot{\delta}_{sw} \\ &+\frac{G_h}{\tau_{d1}\tau_{d2}}[Y_p - (Y + T_p V_x \varphi)] + d_4\end{aligned} \tag{3}$$

where $T_p = \tau_L + \tau_p$ is the preview time; Y_p and $Y+T_pV_x\varphi$ denote the lateral displacement of the desired path preview point and the predicted vehicle position at time $t + \tau_p$.

B. VEHICLE MODEL

As shown in Fig. 2, a two-degree-of-freedom lateral dynamics model schematic diagram of 4WS vehicle is established for controller design.

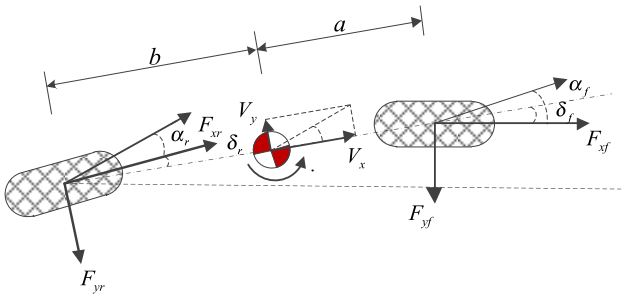

FIGURE 2. Schematic diagram of vehicle model.

Considering vehicle lateral and yaw motions, the motion equations for this model can be described as

$$\begin{cases}\dot{v}_y = -v_x\dot{\varphi} + \dfrac{1}{m}\left(F_{yf} + F_{yr}\right) \\ \ddot{\varphi} = \dfrac{1}{I_z}\left(aF_{yf}\cos\delta_f - bF_{yr}\cos\delta_r\right) \\ \dot{Y} = v_x\sin\varphi + v_y\cos\varphi\end{cases} \tag{4}$$

where m is the total mass of the vehicle; I_z is the vehicle yaw inertia; a and b are the distances from the vehicle center of gravity to the front and rear axles, respectively; v_x, v_y and φ are the vehicle longitudinal velocity, lateral velocity and yaw angle, respectively; δ_f is front tire steering angle and δ_r is rear tire steering angle; F_{yf} and F_{yr} are front and rear lateral tire forces, respectively, which can be defined as

$$\begin{cases}F_{yf} = k_f\alpha_f \\ F_{yr} = k_r\alpha_r\end{cases} \tag{5}$$

where k_f and k_r are the cornering stiffness of the front and rear tires, respectively; α_f, α_r are the slip angles of front and rear tires, respectively, which are described as

$$\begin{cases}\alpha_f = -\delta_f + \dfrac{v_y + a\dot{\varphi}}{v_x} \\ \alpha_r = -\delta_r + \dfrac{v_y - b\dot{\varphi}}{v_x}\end{cases} \tag{6}$$

C. DRIVER-VEHICLE AUGMENTED SYSTEM

Combining the driver model with the vehicle model, a driver-vehicle augmented system is obtained. In order to express the driver-vehicle model in the form of state space, assuming that the front and rear tire steering angle is small and the vehicle heading angle is not large, the equation (4) is rewritten in the following form

$$\begin{cases}\dot{v}_y = -v_x\dot{\varphi} + \dfrac{1}{m}\left(F_{yf} + F_{yr}\right) + d_1 \\ \ddot{\varphi} = \dfrac{1}{I_z}\left(aF_{yf} - bF_{yr}\right) + d_2 \\ \dot{Y} = v_x\varphi + v_y + d_3\end{cases} \tag{7}$$

where

$$\begin{cases}d_1 = \dfrac{1}{m}\left[F_{yf}(\cos\delta_f - 1) + F_{yr}(\cos\delta_r - 1)\right] \\ d_2 = \dfrac{a}{I_z}\left[F_{yf}(\cos\delta_f - 1) - F_{yr}(\cos\delta_r - 1)\right] \\ d_3 = v_x(\sin\varphi - \varphi) + v_y(\cos\varphi - 1)\end{cases} \tag{8}$$

Assuming that the ratio from steering wheel angle to front wheel steering angle is R_g, thus front wheel steering angle can be described as $\delta_f = R_g\delta_{sw}$. $\boldsymbol{x} = \left[v_y\ \dot{\varphi}\ \varphi\ Y\ \delta_{sw}\ \dot{\delta}_{sw}\right]^{\mathrm{T}}$ is the system state vector; $\boldsymbol{w} = \left[Y_p\right]$ is the disturbance input of the system; and $\boldsymbol{u} = [\delta_r]$ is the control input vector to be designed. Combining (3), (5)-(8), the driver-vehicle system model for tracking the desired path can be defined as

$$\begin{cases}\dot{\boldsymbol{x}} = \boldsymbol{A}x + \boldsymbol{B}_1\boldsymbol{w} + \boldsymbol{B}_2\boldsymbol{u} + \boldsymbol{d} \\ \boldsymbol{y} = \boldsymbol{C}x\end{cases} \tag{9}$$

where $\boldsymbol{A}$, $\boldsymbol{B}_1$, $\boldsymbol{B}_2$, $\boldsymbol{d}$, and $\boldsymbol{C}$ as shown at the bottom of the next page.

III. PERSONALIZED CONTROLLER DESIGN

As shown in Fig. 3, the overall control strategy mainly consists of five modules: environmental perception modules, sensor and estimator module, driver model parameter identification module, MPC controller module and rear steering motor module. Environmental perception module perceives the road environment information and gets the desired path Y_p. Driver model parameter identification module identifies the driver parameters according to Y_p, δ_{sw}, $\dot{\varphi}$ and β. Then the target rear wheel angle will send to MPC controller module according to the information obtained from the above modules. Finally, the rear steering motor controls the rear wheel to steer according to the target rear wheel angle. Driver model parameter identification and MPC controller design will be introduced in detailed in the next. Details of analyses about the Environmental perception module and Rear wheel steering motor module are discussed in [24].

A. DRIVER MODEL PARAMETER IDENTIFICATION

In order to facilitate the driver model parameter identification, a simplified closed-loop driver-vehicle system model is established. The block diagram of this system model is shown in Fig. 4.

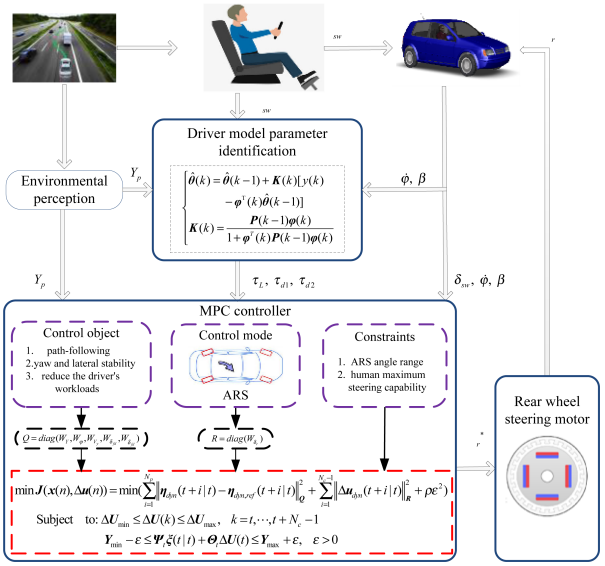

FIGURE 3. Overall control scheme.

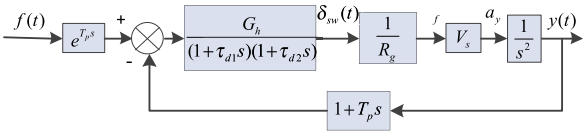

FIGURE 4. Driver preview optimal curvature model diagram structure.

As shown in Fig. 4, the system input signal $f(t)$ stands for the lateral displacement of the desired path and the system output signal $y(t)$ is the lateral displacement of the actual path, $\delta_{sw}(t)$ is the steering wheel angle signal. The V_s denotes the the transfer function between lateral acceleration a_y and front wheel angle δ_f.

The parameters to be identified in the driver model are G_h, τ_{d1} and τ_{d2}. Driver parameters can be identified by desired path signal $f(t)$, actual path signal $y(t)$ and steering wheel angle signal $\delta_{sw}(t)$. From the system block diagram, the equation (10) can be obtained

$$\delta_{sw}(s) = \frac{G_h}{(1+\tau_{d1}s)(1+\tau_{d2}s)}\left(e^{T_p s}f(s) - (1+T_p s)y(s)\right) \tag{10}$$

The transfer function to be identified is

$$G_0(s) = \frac{G_h}{(1+\tau_{d1}s)(1+\tau_{d2}s)} \tag{11}$$

In this study, the recursive least square algorithm is used to identify driver model parameters [24]. Before identifying the parameters, the transfer function $G_0(s)$ should be discretized. The discrete function $G_0(z)$ is as follows

$$G_0(z) = \frac{y(k)}{u(k-1)} = \frac{b_1 z^{-1}}{1 - a_1 z^{-1} - a_2 z^{-2}} \tag{12}$$

where $a_1 = e^{-\frac{T}{\tau_{d1}}} + e^{-\frac{T}{\tau_{d2}}}$; $a_2 = -e^{-(\frac{T}{\tau_{d1}}+\frac{T}{\tau_{d2}})}$; $b_1 = \frac{G_h(e^{-\frac{T}{\tau_{d1}}} - e^{-\frac{T}{\tau_{d2}}})}{\tau_{d1}-\tau_{d2}}$; T is sample time.

$G_0(z)$ can be expressed as controlled auto-regressive model (CAM) as follows

$$A(z^{-1})y(k) = B(z^{-1})u(k-1) + \xi(k) \tag{13}$$

where $\xi(k)$ denotes the white noise signal, and

$$\begin{cases} A(z^{-1}) = 1 - a_1 z^{-1} - a_2 z^{-2} \\ B(z^{-1}) = b_1 z^{-1} \end{cases} \tag{14}$$

The equation (13) can be written in the form of least square.

$$\begin{aligned} y(k) &= a_1 y(k-1) + a_2 y(k-2) + b_1 u(k-2) \\ &= \boldsymbol{\varphi}^T(k)\boldsymbol{\theta} + \boldsymbol{\xi}(k) \end{aligned} \tag{15}$$

$$\boldsymbol{A} = \begin{bmatrix} \frac{k_f + k_r}{m v_x} & -v_x + \frac{a k_f - b k_r}{m v_x} & 0 & 0 & -\frac{R_g k_f}{m} & 0 \\ \frac{a k_f - b k_r}{I_z v_x} & \frac{a^2 k_f + b^2 k_r}{I_z v_x} & 0 & 0 & -\frac{a R_g k_f}{I_z} & 0 \\ 0 & 1 & 0 & 0 & 0 & 0 \\ 1 & 0 & v_x & 0 & 0 & 0 \\ 0 & 0 & 0 & 0 & 0 & 1 \\ 0 & 0 & -\frac{G_h T_p v_x}{\tau_{d1}\tau_{d2}} & -\frac{G_h}{\tau_{d1}\tau_{d2}} & -\frac{1}{\tau_{d1}\tau_{d2}} & -\frac{1}{\tau_{d1}\tau_{d2}} \end{bmatrix};$$

$$\boldsymbol{B}_1 = \begin{bmatrix} 0 & 0 & 0 & 0 & 0 & \frac{G_h}{\tau_{d1}\tau_{d2}} \end{bmatrix}^{\mathrm{T}}; \quad \boldsymbol{B}_2 = \begin{bmatrix} -\frac{k_r}{m} & \frac{b k_r}{I_z} & 0 & 0 & 0 & 0 \end{bmatrix}^{\mathrm{T}};$$

$$\boldsymbol{d} = \begin{bmatrix} d_1 & d_2 & 0 & d_3 & 0 & d_4 \end{bmatrix}^{\mathrm{T}}; \quad \boldsymbol{C} = \begin{bmatrix} 1 & 0 & 0 & 0 & 0 & 0 \\ 0 & 0 & 1 & 0 & 0 & 0 \\ 0 & 0 & 0 & 1 & 0 & 0 \\ 0 & 0 & 0 & 0 & 1 & 0 \\ 0 & 0 & 0 & 0 & 0 & 1 \end{bmatrix}.$$

where $\boldsymbol{\varphi}(k)$ is data vector; $\boldsymbol{\theta}$ is parameter vector to be estimated, and

$$\begin{cases} \boldsymbol{\varphi}(k) = [y(k-1), y(k-2), u(k-2)]^{\mathrm{T}} \\ \boldsymbol{\theta} = [a_1, a_2, b_1]^{\mathrm{T}} \end{cases} \tag{16}$$

According to recursive least square theory, the recursive formula of the estimated parameter vector $\hat{\boldsymbol{\theta}}(k)$ is

$$\begin{cases} \hat{\boldsymbol{\theta}}(k) = \hat{\boldsymbol{\theta}}(k-1) + \boldsymbol{K}(k)[y(k) - \boldsymbol{\varphi}^{\mathrm{T}}(k)\hat{\boldsymbol{\theta}}(k-1)] \\ \boldsymbol{K}(k) = \dfrac{\boldsymbol{P}(k-1)\boldsymbol{\varphi}(k)}{1 + \boldsymbol{\varphi}^{T}(k)\boldsymbol{P}(k-1)\boldsymbol{\varphi}(k)} \\ \boldsymbol{P}(k) = [\boldsymbol{I} - \boldsymbol{K}(k)\boldsymbol{\varphi}^{\mathrm{T}}(k)]\boldsymbol{P}(k-1) \end{cases} \tag{17}$$

After the parameters a_1, a_2 and b_1 are obtained, the identified results can be used to calculate the parameters G_h, τ_{d1}, τ_{d2}.

In order to collect the data needed for driver parameter identification, the driving experiment is carried out on hardware-in-the-loop simulation platform. The experiment scene is double lane-change trajectory and the speed is 15m/s. The results of parameter identification are shown in Fig. 5.

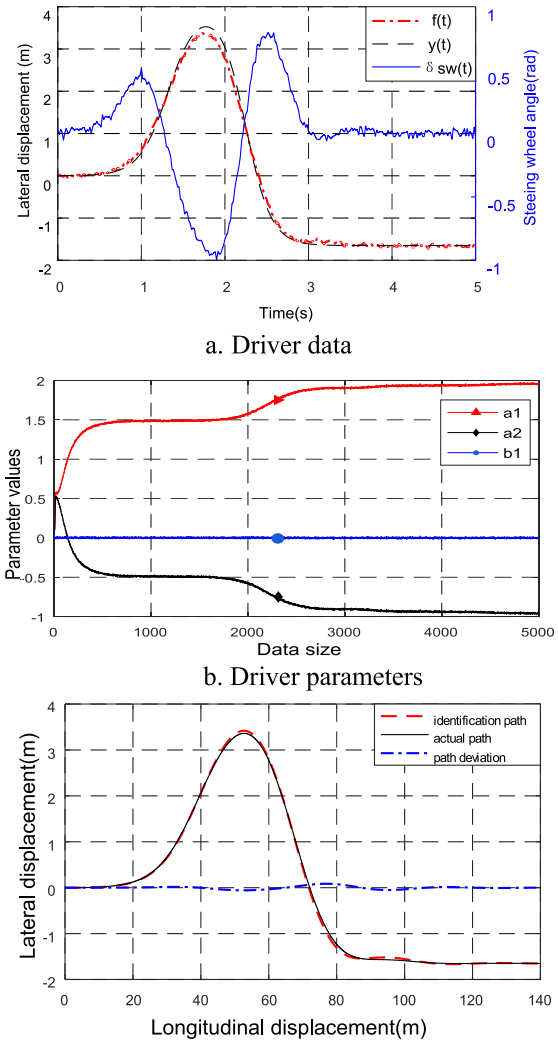

a. Driver data

b. Driver parameters

c. Path

FIGURE 5. Results of parameter identification.

The Fig. 5(a) shows the driver data including the lateral displacement of the desired path $f(t)$, the actual path $y(t)$, and the steering wheel angle signal $\delta_{sw}(t)$. The Fig. 5(b) gives the change curve of driver parameters in the recursive process. After the recursive operation of 4000 sample data, the values of each parameter tend to converge. To verify the accuracy of the driver model parameters identified, the path obtained by the driver model through Matlab/simulink simulation is used to compare with the path measured by the experiment. As shown in Fig. 5(c), the path obtained by the driver model matches the measured path pretty well.

B. MPC CONTROLLER DESIGN

In this section, the path tracking control for ARS vehicles considering driver steering characteristics is formulated as an optimization problem under constraints.

For the design of MPC controller, the continuous-time system model (9) is discretized at a sample time of T_s, then the discrete-time system model can be described as follows [24]:

$$\begin{cases} \boldsymbol{x}(k+1) = \boldsymbol{A}_{k,t}\boldsymbol{x}(k) + \boldsymbol{B}_{1k,t}\boldsymbol{w}(k) + \boldsymbol{B}_{2k,t}\boldsymbol{u}(k) \\ \boldsymbol{y}(k) = \boldsymbol{C}_{k,t}\boldsymbol{x}(k) \end{cases} \tag{18}$$

where, $\boldsymbol{A}_{k,t} = e^{\boldsymbol{A}T_s}, \boldsymbol{B}_{1k,t} = \boldsymbol{B}_1 \int_0^{T_s} e^{\boldsymbol{A}\tau} d\tau, \boldsymbol{B}_{2k,t} = \boldsymbol{B}_2 \int_0^{T_s} e^{\boldsymbol{A}\tau} d\tau, \boldsymbol{C}_{k,t} = \boldsymbol{C}$.

For the convenience of implementing the constraints on the actuator's actuation rate and system state responses simultaneously, a new state variable $\boldsymbol{\xi}(k)$ is introduced to augment the original system state variable at time k, which can be described as

$$\boldsymbol{\xi}(k|t) = \begin{bmatrix} \boldsymbol{x}(k|t) \\ \boldsymbol{u}(k-1|t) \end{bmatrix} \tag{19}$$

Then, the discrete-time system model (10) can be rewritten as

$$\begin{cases} \boldsymbol{\xi}(k+1|t) = \tilde{\boldsymbol{A}}_k\boldsymbol{\xi}(k|t) + \tilde{\boldsymbol{B}}_{1k}\boldsymbol{w}(k|t) + \tilde{\boldsymbol{B}}_{2k}\Delta\boldsymbol{u}(k|t) \\ \boldsymbol{\eta}(k|t) = \tilde{\boldsymbol{C}}_{k,t}\xi(k|t) \end{cases} \tag{20}$$

where $\tilde{\boldsymbol{A}}_{k,t} = \begin{bmatrix} \boldsymbol{A}_{k,t} & \boldsymbol{B}_{2k,t} \\ \boldsymbol{0}_{1\times 6} & \boldsymbol{I}_1 \end{bmatrix}, \tilde{\boldsymbol{B}}_{1k,t} = \begin{bmatrix} \boldsymbol{B}_{1k,t} \\ \boldsymbol{0}_1 \end{bmatrix}, \tilde{\boldsymbol{B}}_{2k,t} = \begin{bmatrix} \boldsymbol{B}_{2k,t} \\ \boldsymbol{I}_1 \end{bmatrix}, \tilde{\boldsymbol{C}}_{k,t} = \begin{bmatrix} \boldsymbol{C}_{k,t} & \boldsymbol{0}_1 \end{bmatrix}$

In addition, to improve computational efficiency and control system real-time property in implementation, it is supposed that $\tilde{\boldsymbol{A}}_{k,t} = \tilde{\boldsymbol{A}}_t, \tilde{\boldsymbol{B}}_{1k,t} = \tilde{\boldsymbol{B}}_{1t}, \tilde{\boldsymbol{B}}_{2k,t} = \tilde{\boldsymbol{B}}_{2t}$ and $\tilde{\boldsymbol{C}}_{k,t} = \tilde{\boldsymbol{C}}_t, k = 1, \cdots, t+N-1$.

In this paper, the prediction horizon is set as N_p and the control horizon is set as N_c. Then the prediction state matrix and output matrix in the prediction horizon can be expressed with the current state and the future control input.

$$\begin{aligned} \boldsymbol{\xi}(t+1|t) &= \tilde{\boldsymbol{A}}_t\boldsymbol{\xi}(t|t) + \tilde{\boldsymbol{B}}_{2t}\Delta\boldsymbol{u}(t|t) + \tilde{\boldsymbol{B}}_{1t}\boldsymbol{w}(t|t) \\ \boldsymbol{\xi}(t+2|t) &= \tilde{\boldsymbol{A}}_t^2\boldsymbol{\xi}(t+1|t) + \tilde{\boldsymbol{A}}_t\tilde{\boldsymbol{B}}_{2t}\Delta\boldsymbol{u}(t|t) \\ &\quad + \tilde{\boldsymbol{B}}_{2t}\Delta\boldsymbol{u}(t+1|t) + \tilde{\boldsymbol{A}}_t\tilde{\boldsymbol{B}}_{1t}\boldsymbol{w}(t|t) \\ &\quad + \tilde{\boldsymbol{B}}_{1t}\boldsymbol{w}(t+1|t) \\ &\vdots \end{aligned}$$

$$\begin{aligned}\boldsymbol{\xi}(t+N_p|t) &= \tilde{\boldsymbol{A}}_t^{N_p}\boldsymbol{\xi}(t+1|t)+\tilde{\boldsymbol{A}}_t^{N_p-1}\tilde{\boldsymbol{B}}_{2t}\Delta\boldsymbol{u}(t|t)\\ &\quad+\cdots+\tilde{\boldsymbol{A}}_t^{N_p-N_c-1}\tilde{\boldsymbol{B}}_{2t}\Delta\boldsymbol{u}(t+N_c|t)\\ &\quad+\tilde{\boldsymbol{A}}_t^{N_p-1}\tilde{\boldsymbol{B}}_{1t}\boldsymbol{w}(t|t)+\cdots+\tilde{\boldsymbol{B}}_{1t}\boldsymbol{w}(t+N_c|t)\\ \boldsymbol{\eta}(t+N_p|t) &= \tilde{\boldsymbol{C}}_t\tilde{\boldsymbol{A}}_t^{N_p}\boldsymbol{\xi}(t+1|t)+\tilde{\boldsymbol{C}}_t\tilde{\boldsymbol{A}}_t^{N_p-1}\tilde{\boldsymbol{B}}_{2t}\Delta\boldsymbol{u}(t|t)\\ &\quad+\cdots+\tilde{\boldsymbol{C}}_t\tilde{\boldsymbol{A}}_t^{N_p-N_c-1}\tilde{\boldsymbol{B}}_{2t}\Delta\boldsymbol{u}(t+N_c|t)\\ &\quad+\tilde{\boldsymbol{C}}_t\tilde{\boldsymbol{A}}_t^{N_p-1}\tilde{\boldsymbol{B}}_{1t}\boldsymbol{w}(t|t)+\cdots\\ &\quad+\tilde{\boldsymbol{C}}_t\tilde{\boldsymbol{A}}_t^{N_p-N_c-1}\tilde{\boldsymbol{B}}_{1t}\boldsymbol{w}(t+N_c|t)\end{aligned}\tag{21}$$

To make the whole relationship more explicit, the output in the prediction horizon is expressed in the form of matrix

$$\boldsymbol{Y}(t)=\boldsymbol{\Psi}_t\boldsymbol{\xi}(t|t)+\boldsymbol{\Theta}_t\Delta\boldsymbol{U}(t)+\boldsymbol{\Phi}_t\boldsymbol{W}(t)\tag{22}$$

where,

$$\boldsymbol{Y}(t)=\left[\boldsymbol{\eta}(t+1|t)\ \ \boldsymbol{\eta}(t+2|t)\ \cdots\ \boldsymbol{\eta}(t+N_c|t)\ \cdots\ \boldsymbol{\eta}(t+N_p|t)\right]^{\mathrm{T}};$$

$$\boldsymbol{\Psi}_t=\left[\tilde{\boldsymbol{C}}_t\tilde{\boldsymbol{A}}_t\ \ \tilde{\boldsymbol{C}}_t\tilde{\boldsymbol{A}}_t^2\ \cdots\ \tilde{\boldsymbol{C}}_t\tilde{\boldsymbol{A}}_t^{N_c}\ \cdots\ \tilde{\boldsymbol{C}}_t\tilde{\boldsymbol{A}}_t^{N_p}\right]^{\mathrm{T}};$$

$$\Delta\boldsymbol{U}(t)=\left[\Delta\boldsymbol{u}(t|t)\ \ \Delta\boldsymbol{u}(t+1|t)\ \cdots\ \Delta\boldsymbol{u}(t+N_c|t)\right]^{\mathrm{T}};$$

$$\boldsymbol{W}(t)=\left[\boldsymbol{w}(t|t)\ \ \boldsymbol{w}(t+1|t)\ \cdots\ \boldsymbol{w}(t+N_c|t)\right]^{\mathrm{T}};$$

$$\boldsymbol{\Theta}_t=\begin{bmatrix}\tilde{\boldsymbol{C}}_t\tilde{\boldsymbol{B}}_{2t} & \boldsymbol{0} & \boldsymbol{0} & \boldsymbol{0}\\ \tilde{\boldsymbol{C}}_t\tilde{\boldsymbol{A}}_t\tilde{\boldsymbol{B}}_{2t} & \tilde{\boldsymbol{C}}_t\tilde{\boldsymbol{B}}_{2t} & \boldsymbol{0} & \boldsymbol{0}\\ \cdots & \cdots & \ddots & \cdots\\ \tilde{\boldsymbol{C}}_t\tilde{\boldsymbol{A}}_t^{N_c-1}\tilde{\boldsymbol{B}}_{2t} & \tilde{\boldsymbol{C}}_t\tilde{\boldsymbol{A}}_t^{N_c-2}\tilde{\boldsymbol{B}}_{2t} & \cdots & \tilde{\boldsymbol{C}}_t\tilde{\boldsymbol{B}}_{2t}\\ \tilde{\boldsymbol{C}}_t\tilde{\boldsymbol{A}}_t^{N_c}\tilde{\boldsymbol{B}}_{2t} & \tilde{\boldsymbol{C}}_t\tilde{\boldsymbol{A}}_t^{N_c-1}\tilde{\boldsymbol{B}}_{2t} & \cdots & \tilde{\boldsymbol{C}}_t\tilde{\boldsymbol{A}}_t\tilde{\boldsymbol{B}}_{2t}\\ \vdots & \vdots & \ddots & \vdots\\ \tilde{\boldsymbol{C}}_t\tilde{\boldsymbol{A}}_t^{N_p-1}\tilde{\boldsymbol{B}}_{2t} & \tilde{\boldsymbol{C}}_t\tilde{\boldsymbol{A}}_t^{N_p-2}\tilde{\boldsymbol{B}}_{2t} & \cdots & \tilde{\boldsymbol{C}}_t\tilde{\boldsymbol{A}}_t^{N_p-N_c-1}\tilde{\boldsymbol{B}}_{2t}\end{bmatrix};$$

$$\boldsymbol{\Phi}_t=\begin{bmatrix}\tilde{\boldsymbol{C}}_t\tilde{\boldsymbol{B}}_{1t} & \boldsymbol{0} & \boldsymbol{0} & \boldsymbol{0}\\ \tilde{\boldsymbol{C}}_t\tilde{\boldsymbol{A}}_t\tilde{\boldsymbol{B}}_{1t} & \tilde{\boldsymbol{C}}_t\tilde{\boldsymbol{B}}_{1t} & \boldsymbol{0} & \boldsymbol{0}\\ \cdots & \cdots & \ddots & \cdots\\ \tilde{\boldsymbol{C}}_t\tilde{\boldsymbol{A}}_t^{N_c-1}\tilde{\boldsymbol{B}}_{1t} & \tilde{\boldsymbol{C}}_t\tilde{\boldsymbol{A}}_t^{N_c-2}\tilde{\boldsymbol{B}}_{1t} & \cdots & \tilde{\boldsymbol{C}}_t\tilde{\boldsymbol{B}}_{1t}\\ \tilde{\boldsymbol{C}}_t\tilde{\boldsymbol{A}}_t^{N_c}\tilde{\boldsymbol{B}}_{1t} & \tilde{\boldsymbol{C}}_t\tilde{\boldsymbol{A}}_t^{N_c-1}\tilde{\boldsymbol{B}}_{1t} & \cdots & \tilde{\boldsymbol{C}}_t\tilde{\boldsymbol{A}}_t\tilde{\boldsymbol{B}}_{1t}\\ \vdots & \vdots & \ddots & \vdots\\ \tilde{\boldsymbol{C}}_t\tilde{\boldsymbol{A}}_t^{N_p-1}\tilde{\boldsymbol{B}}_{1t} & \tilde{\boldsymbol{C}}_t\tilde{\boldsymbol{A}}_t^{N_p-2}\tilde{\boldsymbol{B}}_{1t} & \cdots & \tilde{\boldsymbol{C}}_t\tilde{\boldsymbol{A}}_t^{N_p-N_c-1}\tilde{\boldsymbol{B}}_{1t}\end{bmatrix}.$$

Considering the multi-objectives including path-tracking error, vehicle stability, driver's physical workloads, mental workloads and the control effort, according to LQR control method, the cost function is defined as

$$J=\int_0^\infty\left[q_1v_y^2+q_2(\varphi_d-\varphi)^2+q_3(Y_d-Y)^2+q_4\delta_{sw}^2+q_5\dot{\delta}_{sw}^2+R\Delta\delta_r^2\right]dt\tag{23}$$

where $q_i(i=1,2,3,4,5)$ and R are weighting factors, $J_1=\int_0^\infty(Y_d-Y)^2dt$ and $J_2=\int_0^\infty(\varphi_d-\varphi)^2dt$ represent the assessment of the path-tracking performance; φ_d and Y_d denote the reference heading angle and the reference lateral position of current time, respectively; $J_3=\int_0^\infty v_y^2dt$ denotes the vehicle stability performance; $J_4=\int_0^\infty\delta_{sw}^2dt$ and $J_5=\int_0^\infty\dot{\delta}_{sw}^2dt$ describe the driver's physical and mental workloads [41]–[43], respectively; $J_6=\int_0^\infty\Delta\delta_r^2dt$ represents the steering rate of the rear wheel. Equation (16) can be rewritten as

$$\begin{aligned}J(\boldsymbol{\xi}(t),\boldsymbol{u}(t-1),\Delta\boldsymbol{U}(t)) &= \sum_{i=1}^{N_p}\left\|\boldsymbol{\eta}(t+i|t)-\boldsymbol{\eta}_{\mathrm{ref}}(t+i|t)\right\|_Q^2\\ &\quad+\sum_{i=1}^{N_p-1}\|\Delta\boldsymbol{u}(t+i|t)\|_R^2+\rho\varepsilon^2\end{aligned}\tag{24}$$

where ρ is weighting coefficient; ε is relaxation factor; $\boldsymbol{Q}=diag\left[q_1\ q_2\ q_3\ q_4\ q_5\right]$; $\boldsymbol{\eta}_{\mathrm{ref}}=\left[0\ \varphi_d\ Y_d\ 0\ 0\right]^{\mathrm{T}}$; $\Delta\boldsymbol{u}=[\Delta\delta_r]$.

The output deviation in the prediction time domain are

$$\boldsymbol{E}(t)=\boldsymbol{\Psi}_t\tilde{\boldsymbol{\xi}}(t|t)+\boldsymbol{\Phi}_t\boldsymbol{W}(t)-\boldsymbol{Y}_{\mathrm{ref}}(t),\tag{25}$$

$$\boldsymbol{Y}_{\mathrm{ref}}=[\eta_{\mathrm{ref}}(t+1|t),\cdots\eta_{\mathrm{ref}}(t+N_p|t)]^{\mathrm{T}}\tag{26}$$

The cost function (17) can be adjusted as

$$\begin{aligned}J(\boldsymbol{\xi}(t),\boldsymbol{u}(t-1),\Delta\boldsymbol{U}(t)) &= \left[\Delta\boldsymbol{U}(t)^{\mathrm{T}},\varepsilon\right]^{\mathrm{T}}\boldsymbol{H}_t\left[\Delta\boldsymbol{U}(t)^{\mathrm{T}},\varepsilon\right]\\ &\quad+\boldsymbol{G}_t\left[\Delta\boldsymbol{U}(t)^{\mathrm{T}},\varepsilon\right]+P_t\end{aligned}\tag{27}$$

where $\boldsymbol{H}_t=\begin{bmatrix}\boldsymbol{\Theta}_t^{\mathrm{T}}\boldsymbol{Q}_e\boldsymbol{\Theta}_t^{\mathrm{T}}+\boldsymbol{R}_e & \boldsymbol{0}\\ \boldsymbol{0} & \rho\end{bmatrix}$; $\boldsymbol{G}_t=\left[2\boldsymbol{E}(t)^{\mathrm{T}}\boldsymbol{Q}_e\boldsymbol{\Theta}_t\ \ 0\right]$; $P_t=\boldsymbol{E}(t)^{\mathrm{T}}\boldsymbol{Q}_e\boldsymbol{E}(t)$, P_t is a constant.

In real practice, there are some physical constrains for this optimization problem for both output and control variables.

The control input increment $\Delta\boldsymbol{u}=[\Delta\delta_r]$ and the control input $\mathbf{u}=[\delta_r]$ represent the speed and amplitude the rear steering wheel angle, so they both should obey the physical limits of the actuators, which could be expressed as

$$\begin{cases}\Delta\boldsymbol{U}_{\min}\le\Delta\boldsymbol{U}(k)\le\Delta\boldsymbol{U}_{\max},k=t,\\ \quad t+1,\cdots,t+N_c-1\\ \boldsymbol{U}_{\min}\le\boldsymbol{u}(t-1)+\sum_{i=t}^{k}\Delta\boldsymbol{U}(k)\le\boldsymbol{U}_{\max},k=t,\\ \quad t+1,\cdots,t+N_c-1\end{cases}\tag{28}$$

where $\Delta\boldsymbol{U}_{\min}$ $\Delta\boldsymbol{U}_{\min}$ and $\Delta\boldsymbol{U}_{\max}$ denote the lower and upper limits for control input increments vector $\Delta\boldsymbol{U}_k$, respectively; $\boldsymbol{U}_{\min}$ and $\boldsymbol{U}_{\max}$ represent the lower and upper limits for control input vector $\boldsymbol{U}_k$, respectively.

For the safety and stability of the vehicle and considering the steering wheel angle δ_{sw} and steering rate $\dot{\delta}_{sw}$ limits, the output also should be limited. This constraint can be written as

$$\begin{aligned}\boldsymbol{Y}_{\min}-\varepsilon &\le \boldsymbol{\Psi}_t\boldsymbol{\xi}(t|t)+\boldsymbol{\Theta}_t\Delta\boldsymbol{U}(t)+\boldsymbol{\Phi}_t\boldsymbol{W}(t)\\ &\le \boldsymbol{Y}_{\max}+\varepsilon,\varepsilon>0\end{aligned}\tag{29}$$

With all the constraints above, the optimization problem can be summerized as

$$\min_{\Delta U_t,\varepsilon} \left[\Delta \boldsymbol{U}(t)^{\mathrm{T}}, \varepsilon\right]^{\mathrm{T}} \boldsymbol{H}_t \left[\Delta \boldsymbol{U}(t)^{\mathrm{T}}, \varepsilon\right] + \boldsymbol{G}_t \left[\Delta \boldsymbol{U}(t)^{\mathrm{T}}, \varepsilon\right] \tag{30}$$

subject to

$$\begin{cases} \Delta \boldsymbol{U}_{\min} \le \Delta \boldsymbol{U}(k) \le \Delta \boldsymbol{U}_{\max}, k = t, \\ \quad t+1, \cdots, t+N_c-1 \\ \boldsymbol{U}_{\min} \le \boldsymbol{u}(t-1) + \sum_{i=t}^{k} \Delta \boldsymbol{U}(k) \le \boldsymbol{U}_{\max}, k = t, \\ \quad t+1, \cdots, t+N_c-1 \\ \boldsymbol{Y}_{\min} - \varepsilon \le \boldsymbol{\Psi}_t \boldsymbol{\xi}(t|t) + \boldsymbol{\Theta}_t \Delta \boldsymbol{U}(t) + \boldsymbol{\Phi}_t \boldsymbol{W}(t) \\ \quad \le \boldsymbol{Y}_{\max} + \varepsilon \\ \varepsilon > 0 \end{cases} \tag{31}$$

By solving the proposed constrained optimization problem with Matlab, the sequence of the optimal input increments can be obtained

$$\Delta \boldsymbol{U}_t^* = [\Delta \boldsymbol{u}_t^*, \Delta \boldsymbol{u}_{t+1}^*, \cdots, \Delta \boldsymbol{u}_{t+N_c-1}^*]^{\mathrm{T}} \tag{32}$$

The first sample of $\Delta \boldsymbol{u}_t^*$ is used to compute the optimal steering torque control law

$$\boldsymbol{u}(t) = \boldsymbol{u}(t-1) + \Delta \boldsymbol{u}_t^* \tag{33}$$

IV. SIMULATION STUDIES

In order to verify the effectiveness of the proposed control strategy, simulations are executed by using the co-simulation platform of CarSim and Matlab/simulink. Two driver models with different parameters are identified in advance. The Driver A is an experienced and aggressive driver with smaller time delay and larger steering proportional gain, while Driver B is an inexperienced driver with longer time delay and smaller steering proportional gain. The MPC controllers are designed for each driver, respectively. In controller design, the maximum allowable deviation of trajectory tracking as well as the maximum human capability of steering angle and steering rate constraints are set based on the data given in [25].

Five quadratic integral functions are adopted to evaluate the performance and steering work loads of a driver [26]. The parameters of the drivers and vehicle are shown in Table 1 and Table 2.

TABLE 1. Parameters of drivers.

Parameter	τ_L	τ_{d1}	τ_{d2}	τ_p	G_h
DA	0.1	0.05	0.08	0.8	1.0
DB	0.1	0.085	0.15	0.65	0.6

In order to verify the effectiveness of the proposed controller for driving assistance, let Driver A and Driver B drive the vehicle with and without the controller, respectively, and their simulation results are compared. The driving condition is set as double lane-change trajectory with constant vehicle speed of 15 m/s. The simulation results are shown in Fig. 6.

TABLE 2. Parameters of vehicle.

Parameter	Meaning	Value
m	Vehicle total mass	1259.98 kg
I_z	Vehicle yaw moment of inertia	4607 kgm^2
a	Distance from CG to front axle	1.14 m
b	Distance from CG to rear axle	1.64 m
k_f	Cornering stiffness of the front tire	-143583 Nrad
k_r	Cornering stiffness of the rear tire	-111200 Nrad
R_g	Transmission ratio of steering system	1/17

It can be seen from Fig. 6 that, when the controller is not applied, the inexperienced Driver B has greater steering wheel angle and steering wheel angle rate than the experienced Driver A. Thus the response of yaw rate and sideslip angle of the vehicle driven by Driver B are greater than that of the vehicle driven by Driver A, and the deviation of path tracking is larger.

In case the controller is applied, steering wheel angle and steering wheel angle rate of the vehicle driven by Driver A and B both decrease compared with that of the controller is not applied, and the reduction of Driver B is more obvious. As a result, the driver's physical workload and mental workload are all reduced. Fig. 6.c show the vehicle's rear wheel angle under the work of the proposed controller. Under the work of the controller, the rear wheel steering direction of the vehicle driven by experienced Driver A is the same as the front wheel, while the direction of the vehicle driven by inexperienced Driver B is opposite to the front wheel, so as to better track the target path. In case of vehicle stability, when the controller is applied, the sideslip angle are both reduced compared with that of the controller is not applied. Thus, the stability of the vehicle is improved. In the aspect of path tracking control, compared with no control, the path deviation of the two drivers' driving vehicles is reduced, and the improvement effect of the inexperienced Driver B is more obvious.

It can be seen in Table 3 that, when the controller is not applied, the task performance, physical workload and mental workload of Driver A are all smaller than those of Driver B. However, when the controller is applied, the three indicators of Driver A and Driver B are all decreased, and the workload of Driver B become smaller than those of Driver A. This means the proposed controller can significantly improve the driver's task performance, decrease the driver's workload.

TABLE 3. Control performance.

	J_1	J_2	J_3	J_4	J_5
DA	0.021	0.015	0.978	3.40-03	0.014
DA+CA	0.014	0.0117	0.085	1.40e-03	6.43-03
DB	0.061	0.0167	0.465	9.89e-03	0.040
DB+CB	0.0118	0.0103	0.163	1.15e-03	4.63e-03

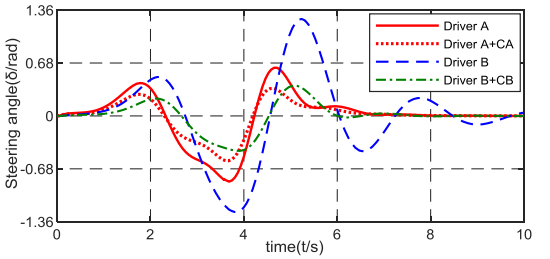

a. Steering wheel angle

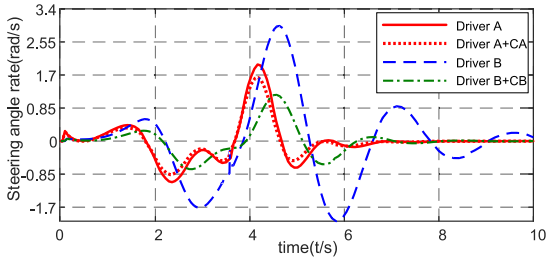

b. Steering wheel angle rate

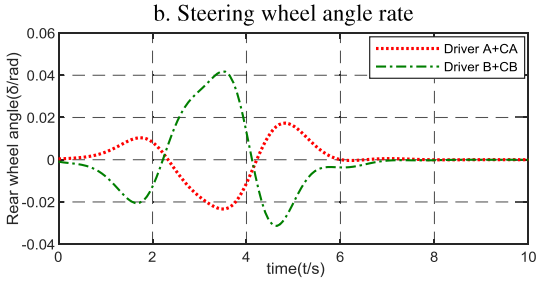

c. Rear wheel angle

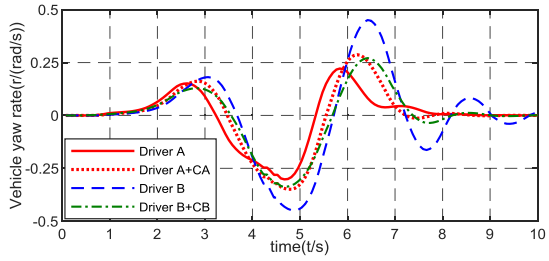

d. Vehicle yaw rate

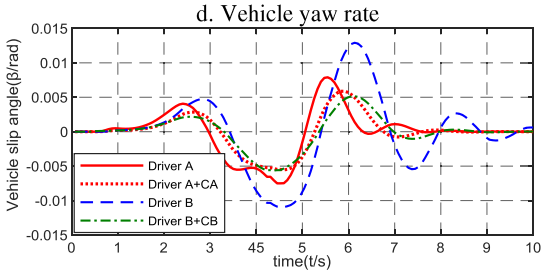

e. Side slip angle

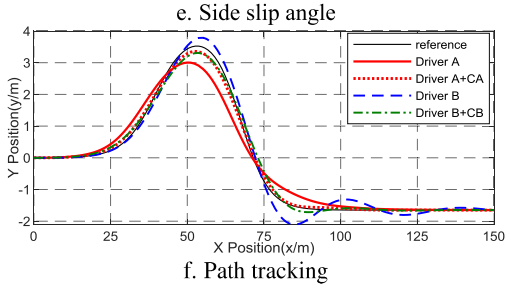

f. Path tracking

FIGURE 6. Simulation results.

V. CONCLUSIONS

A path tracking control strategy for active rear steering considering driver steering characteristics is proposed in this paper. The driver-vehicle augmented system is established based on driver and vehicle model at first. The driver characteristics are identified based on daily driving data, then the MPC control algorithm considering the task performance, vehicle stability, driver's physical workloads, mental workloads and actuator performance, is designed to optimize the overall performance of the driver-vehicle system. The simulation results prove that the personalized controller can significantly improve the system performance and reduce the driver's workloads.

REFERENCES

[1] N. C. Basjaruddin, Kuspriyanto, Suhendar, D. Saefudin, and S. A. Aryani, "Lane keeping assist system based on fuzzy logic," in *Proc. Int. Electron. Symp. (IES)*, Sep. 2015, pp. 110–113.
[2] J. Guo, Y. Luo, C. Hu, C. Tao, and K. Li, "Robust combined lane keeping and direct yaw moment control for intelligent electric vehicles with time delay," *Int. J. Automot. Technol.*, vol. 20, no. 2, pp. 289–296, Apr. 2019.
[3] Y. J. Liu, Y. Q. Zhao, and X. F. Zhou, "Design research on vehicle collision avoidance based on artificial potential field," *Appl. Mech. Mater.*, vol. 271, pp. 727–731, 2013.
[4] J. Minguez and L. Montano, "Extending collision avoidance methods to consider the vehicle shape, kinematics, and dynamics of a mobile robot," *IEEE Trans. Robot.*, vol. 25, no. 2, pp. 367–381, Apr. 2009.
[5] J. Ji, A. Khajepour, W. W. Melek, and Y. Huang, "Path planning and tracking for vehicle collision avoidance based on model predictive control with multiconstraints," *IEEE Trans. Veh. Technol.*, vol. 66, no. 2, pp. 952–964, Feb. 2017.
[6] N. Nakrani and M. Joshi, "An intelligent fuzzy based hybrid approach for parallel parking in dynamic environment," *Procedia Comput. Sci.*, vol. 133, pp. 82–91, Jan. 2018.
[7] E. Jelavic, J. Gonzales, and F. Borrelli, "Autonomous drift parking using a switched control strategy with onboard sensors," *IFAC-PapersOnLine*, vol. 50, no. 1, pp. 3714–3719, Jul. 2017.
[8] A. Goodarzi and M. Ghajar, "Integrating lane-keeping system with direct yaw moment control tasks in a novel driver assistance system," *Proc. Inst. Mech. Eng., K, J. Multi-Body Dyn.*, vol. 229, no. 1, pp. 16–38, Mar. 2015.
[9] C. Wnag, W. Zhao, Z. Xu, and G. Zhou, "Path planning and stability control of collision avoidance system based on active front steering," *Sci. China Technol. Sci.*, vol. 60, no. 8, pp. 1231–1243, Aug. 2017.
[10] S. Salehpour, Y. Pourasad, and S. H. Taheri, "Vehicle path tracking by integrated chassis control," *J. Central South Univ.*, vol. 22, no. 4, pp. 1378–1388, Apr. 2015.
[11] Z. Lin, X. Jiao, and Z. Wang, "ADRC-based active front steering strategy for path tracking of a farm vehicle," in *Proc. 3rd Conf. Vehicle Control Intell. (CVCI)*, Hefei, China, Sep. 2019, pp. 1–5.
[12] R. L. Roebuck, A. M. Odhams, and D. Cebon, "An automatically reconfigurable software-based safety system for rear-steering multi-unit vehicles," *Proc. Inst. Mech. Eng., D, J. Automobile Eng.*, vol. 229, no. 2, pp. 143–162, Feb. 2015.
[13] B. Zhang, A. Khajepour, and A. Goodarzi, "Vehicle yaw stability control using active rear steering: Development and experimental validation," *Proc. Inst. Mech. Eng., K, J. Multi-Body Dyn.*, vol. 231, no. 2, pp. 333–345, Jun. 2017.
[14] M. Völker and W. Stadie, "Electrohydraulic rear axle steering systems for agricultural vehicles," *ATZoffhighway Worldwide*, vol. 10, no. 4, pp. 22–27, Nov. 2017.
[15] C. Alexandru, "A mechanical integral steering system for increasing the stability and handling of motor vehicles," *Proc. Inst. Mech. Eng., C, J. Mech. Eng. Sci.*, vol. 231, no. 8, pp. 1465–1480, Apr. 2017.
[16] B. Li, S. Rakheja, and Y. Feng, "Enhancement of vehicle stability through integration of direct yaw moment and active rear steering," *Proc. Inst. Mech. Eng., D, J. Automobile Eng.*, vol. 230, no. 6, pp. 830–840, May 2016.

[17] Y. Zhang, A. Khajepour, and X. Xie, "Rollover prevention for sport utility vehicles using a pulsed active rear-steering strategy," *Proc. Inst. Mech. Eng., D, J. Automobile Eng.*, vol. 230, no. 9, pp. 1239–1253, Aug. 2016.
[18] G. Li, S. Eben Li, and B. Cheng, "Field operational test of advanced driver assistance systems in typical chinese road conditions: The influence of driver gender, age and aggression," *Int. J. Automot. Technol.*, vol. 16, no. 5, pp. 739–750, Oct. 2015.
[19] M. Flad, C. Trautmann, G. Diehm, and S. Hohmann, "Individual driver modeling via optimal selection of steering primitives," *IFAC Proc. Vols.*, vol. 47, no. 3, pp. 6276–6282, 2014.
[20] L. Saleh, P. Chevrel, F. Mars, J.-F. Lafay, and F. Claveau, "Human-like cybernetic driver model for lane keeping," *IFAC Proc. Vols.*, vol. 44, no. 1, pp. 4368–4373, Jan. 2011.
[21] J. M. Choi, S.-Y. Liu, and J. K. Hedrick, "Human driver model and sliding mode control–road tracking capability of the vehicle model," in *Proc. Eur. Control Conf. (ECC)*, Jul. 2015, pp. 2132–2137.
[22] F. Wang, H. Chen, and D. Cao, "Nonlinear coordinated motion control of road vehicles after a tire blowout," *IEEE Trans. Control Syst. Technol.*, vol. 24, no. 3, pp. 956–970, May 2016.
[23] M. Plöchl and J. Edelmann, "Driver models in automobile dynamics application," *Vehicle Syst. Dyn.*, vol. 45, nos. 7–8, pp. 699–741, Jul. 2007.
[24] Y. Sun, B. Jing, and J. Zhang, "Multi-sensor information fusion based on the combination of optimal weight and recursive least square algorithm," *J. Transcluction Technol.*, vol. 17, no. 4, pp. 629–630, 2004.
[25] S. Taheri, S. Rakheja, and H. Hong, "Influence of human driving characteristics on path tracking performance of vehicle," in *Intelligent Robotics and Applications*. Berlin, Germany: Springer-Verlag, 2012, pp. 207–216.
[26] P. Bolia, T. Weiskircher, and S. Müller, "Driver steering model for closed-loop steering function analysis," *Vehicle Syst. Dyn.*, vol. 52, no. 1, pp. 16–30, May 2014.

HAN ZHANG received the B.S. degree in vehicle engineering from the Nanjing University of Aeronautics and Astronautics, Nanjing, China, in 2014, where she is currently pursuing the Ph.D. degree with the Department of Vehicle Engineering. Her research interests include vehicle system dynamics and control systems.

BO HENG is currently pursuing the Graduate degree with the Department of Vehicle Engineering, Nanjing University of Aeronautics and Astronautics, Nanjing, China. His research interest includes vehicle system dynamics.

WANZHONG ZHAO is currently a Professor and the Director of the Department of Vehicle Engineering, Nanjing University of Aeronautics and Astronautics, Nanjing, China. His research interest includes vehicle system dynamics.